CHEMPHYSCHEM

Supporting Information

Force Distribution Analysis of Mechanochemically Reactive Dimethylcyclobutene

Wenjin Li,[a, b] Scott A. Edwards,[c] Lanyuan Lu,[d] Tomas Kubar,[e] Sandeep P. Patil,[f] Helmut Grubmüller,[b] Gerrit Groenhof,*[b, g] and Frauke Gräter*[a, f]

cphc_201300252_sm_miscellaneous_information.pdf

Force Matching-Force Distribution Analysis (FM-FDA)

Construction of a pairwise force field by MSCGFM

To construct a pairwise force field (PWFF) for trans-3,4-dimethylcyclobutene (tDCB), the atoms with similar properties are grouped into the same atom type. For example, carbon atoms CA and CF are symmetric in tDCB and both are part of -CH_3 groups, and thus are defined as C1 type (or CG site). Definitions of other atoms can be found in Table S9

Using the MSCGFM program, we constructed the PWFF from the results of quantum mechanical (QM) simulations.[1] The bonded interactions were defined within atom pairs separated by less than three bonds (1-2, 1-3 and 1-4 atom pairs), the non-bonded interactions were defined between atom pairs separated by three and more bonds. The cut-off for non-bonded interaction was 1.2 nm, and linear spline basis sets were used. All atoms were set to be neutral, i.e., with zero charge.

At the SCC-DFTB (self-consistent-charges density-functional tight-binding[2]) level, ten trajectories, 2 ns each, (400,000 structures in total) were used to construct the PWFF. The resulting PWFF for bonded and non-bonded interactions is shown in Fig. S5. At the O3LYP level, 500 trajectories, 200 fs each, (100,000 structures in total) were used to construct the PWFF.

Force distribution analysis

The tabulated potentials of our PWFF cover only the range of inter-atomic distances sampled in the QM simulations. To cover the whole range of distances potentially sampled, starting from zero to a specific distance (0.4 nm, 0.6 nm and 0.8 nm for 1-2, 1-3 and 1-4 bonded potentials, respectively, 2.4 nm for non-bonded potentials), we assumed a linear potential in the range outside of the bond length sampled in the simulations. For example, Fig. S6 shows the extrapolation of the tabulated potential on C2-C3 to the range from zero to 0.4 nm. Then we performed reruns on the QM trajectories to obtain the force distributions based on the PWFF. Although the assumption of a linear potential is hardly accurate, its effect on the results is minimal since the region outside of the sampled region is rarely visited.

Conformational Flooding

Introduction Conformational flooding is developed to study rare events, such as chemical reactions or slow conformational motions of macromolecules.[3,4] At first, an effective Hamiltonian (H_{Eff}) is constructed to approximate the conformational substates (CS's) of a many-body system. Then, a flooding potential (V_{fl}) is introduced into the Hamiltonian to drive the system out of the CS's.

Since V_{fl} adopts the same shape as H_{Eff}, conformational transitions are accelerated without bias. Assume that V_{fl} does not affect the free energy surface of the transition regions, in other words, V_{fl} meets the criteria of locality and uniformity, the acceleration factor α can be expressed as follows (Eq. (25) in Ref. [2]),

$$\alpha \approx \frac{1}{\langle e^{-\mathrm{V_{fl}/kT}} \rangle_{\mathrm{sk}}} \tag{S1}$$

or

$$\alpha \approx \langle e^{\mathrm{V_{fl}/kT}} \rangle_{\mathrm{sk'}} \tag{S2}$$

Here, $\langle\rangle_{\mathrm{sk}}$ and $\langle\rangle_{\mathrm{sk'}}$ are the averages over sub-canonical ensembles of the system without and with flooding potential, respectively.

Then, the destabilization free energy ΔG^{fl}, which is the decrease in free energy due to the introduction of V_{fl} , is defined as

$$\Delta G^{\mathrm{fl}} \equiv k_{\mathrm{B}} T \cdot \ln\alpha \tag{S3}$$

Therefore, ΔG^{fl} can be estimated by

$$\Delta G^{\mathrm{fl}} = -k_{\mathrm{B}}T \cdot \ln\langle e^{-\mathrm{V_{fl}/kT}}\rangle_{\mathrm{sk}} = k_{\mathrm{B}}T \cdot \ln\langle e^{\mathrm{V_{fl}/kT}}\rangle_{\mathrm{sk'}} \tag{S4}$$

Thus, a consistency between the ΔG^{fl} obtained for the two ensembles is necessary for the locality and uniformity of the flooding potential.

In the case of a chemical reaction, the acceleration factor α is defined by

$$\alpha \equiv \frac{k_0}{k_{\mathrm{fl}}} \tag{S5}$$

where k_0 and k_{fl} are the rates of the reaction with and without flooding potential, respectively. Combining Eq. S5 and Eq. S3, we obtain

$$k_{\mathrm{fl}} = k_0 \cdot \exp(\Delta G^{\mathrm{fl}}/k_{\mathrm{B}}T) \tag{S6}$$

Computational details First we performed 2 ns simulations in equilibrium, and a flooding potential on the six-carbon atoms was built over 100,000 structures from the last 1ns trajectories. We then applied a flooding potential to the tDCB with different flooding strengths, from 30 kJ/mol to 130 kJ/mol. According to Eq. S4, the destabilization free energies ΔG^{fl} in two different ensembles were estimated. The results are shown in Table S10 and Fig. S7. They are consistent with each other, which shows that the flooding potential captures the essential features of the conformational substate of cycobutene.

At high flooding potential strength, e.g., 130 kJ/mol, the two ΔG^{fl}'s slightly differ, and the average of them is taken as the ΔG^{fl} onto tDCB. At a flooding strength of 130 kJ/mol, ΔG^{fl}=115.5 kJ/mol.

In system A, we estimated the rate of ring-opening under forces ranging from 0 pN to 700 pN under flooding strengths of 130 kJ/mol and 125 kJ/mol. The resulting rates are given in Table S1. Fig. S8 shows the obtained rates as a function of the external force. The rates estimated with the two flooding strengths were fitted to Dudko-Hummer model. The fitted parameters are given in Table S11.

Effective forces on tDCB from strained macrocycles

Rate calculations by simulations For a given reaction with rate constant k, the probability of a transition at time t is given as follows,

$$p(t) = -k\exp(-kt) \tag{S7}$$

Thus, the probability of transitions that occur at a time no less than t is given by

$$P(t) = \int_0^{\mathrm{t}} p(t')dt' = 1 - \exp(-kt) \tag{S8}$$

If one runs N independent simulations with a fixed time length of T, there are n simulations in which the reaction occurs, and the times for transition are $t_1, t_2, ..., t_{\mathrm{n}}$. In the other $N - n$ simulations, no transition occurs. Then the maximum likelihood (M) of the event equals,

$$M = \prod_{\mathrm{i}=1}^{\mathrm{n}} p(t_{\mathrm{i}})[1 - P(T)]^{\mathrm{N-n}} \tag{S9}$$

Then, by taking $d\mathrm{ln}M/dk = 0$, we obtain the maximum likelihood estimation of the rate constant k as follows,

$$k = \frac{n}{(N-n)T + \sum_{\mathrm{i}=1}^{\mathrm{n}} t_{\mathrm{i}}} \tag{S10}$$

From Eq. S8, we can also obtain:

$$\ln(1 - P(t)) = -kt \tag{S11}$$

Thus, $\ln(1-P(t))$ is in a linear relationship with t. We thus examined $\ln(1-P(t))$ as a function of t for estimating rates, and straight lines were obtained in all cases, highlighting the accuracy of the rates estimated with conformational flooding. As examples, $\ln(1 - P(t))$ as a function of t in the case of 4Z, 4E, 9Z, and 9E are shown in Fig. S10.

Force-dependent ring-opening kinetics

Rates estimated from experimental data The dependence of the rate on temperature can be described by the Eyring equation,

$$k = \frac{k_{\mathrm{B}}T}{h} \cdot \exp(-\Delta \mathrm{G}^{\ddagger}/\mathrm{RT}) \tag{S12}$$

where k is reaction rate constant, $\Delta G^{\ddagger}$ is the Gibbs energy of activation, k_{B} is Boltzmann's constant, h is Planck's constant, R is gas constant and T is absolute temperature.

It can be written as

$$\ln\frac{k}{T} = \frac{-\Delta H^{\ddagger}}{R} \cdot \frac{1}{T} + \ln\frac{k_{\mathrm{B}}}{h} + \frac{\Delta S^{\ddagger}}{R} \tag{S13}$$

where $\Delta H^{\ddagger}$ is the enthalpy of activation, and $\Delta S^{\ddagger}$ the entropy of activation.

Thus, $\ln\frac{k}{T}$ is in a linear relationship with $\frac{1}{T}$. Here, we took the rates in Supplementary Tables 11 and 12 in the work of Boulatov and coworkers,[5] which were estimated under different temperatures

by experiments, and analyzed $\ln\frac{k}{T}$ as a function of $\frac{1}{T}$. All results could be fitted by lines very well. We then extrapolated the data to a temperature of 300 K, to estimate the rates of ring-opening in each macrocycle at 300 K. The logarithm of the extrapolated rates are shown in Fig. 2B of the main text.

Finite element calculations

In the present study, the S-DYNA 971[6] commercial finite element analysis software was used.

The coordinates of carbon atoms in tDCB (CA to CF) were directly taken from the QM calculations. All nodes (atoms) were connected with beam elements along covalent bonds. A fine mesh was obtained by dividing each beam element between nodes into 6 to 8 elements. The structure was modeled by rigid-jointed, linear-elastic beam elements. For all beams, we defined a Belytschko-Schwer resultant beam[7] (elform=2) with the following properties: a cross-sectional area of 7.85E-05 mm^2; a 2nd moment of area about the s-axis of 4.91E-10 mm^4; a 2nd moment of area about the t-axis of 4.91E-10 mm^4; a 2nd polar moment of area about the beam axis of 9.82E-10 mm^4. As in the QM calculations, the structure was not constrained at any node. Loads were applied on the CA and CF nodes in opposite directions. As material parameters for the beam elements, we chose a density(ρ) of 7.85 g/cm^3; a modulus of elasticity(E) of 210 GPa, and a Poisson's ratio(v) of 0.3. The qualitative stress distribution was independent from the particular choice of these parameters.

We performed FEM simulations on the trans and cis structures, as well as the chemically unfeasible in-plane structure. All FEM simulations show a significant extension, i.e., tensile axial forces, in CB-CE branch, and a compression, i.e., compressive axial forces, in the CC-CD branch. The tensile forces on CA and CF directly transfer to the nodes CB and CE and thereby extend the CB-CE branch. On the other hand, to balance this tensile force, the CC-CD branch gets compressed. The CB-CC and CD-CE branches get compressed with very small magnitude. Due to the linear elasticity, all axial stresses scale linearly with force, so that axial stresses normalized by the external load as shown in Fig. 3B are constant.

Contribution of stressed bonds to increased reaction rates

As explained in the main text, $F_{\mathrm{ext}}\Delta x_{\mathrm{r}}$ is the total work on the system when the external force is lower than 500 pN. Now, we want to decompose this work into the work on individual bonds ($F_{\mathrm{FDA}}\Delta x_{\mathrm{r}}$).

If the sum of the effect of force on several bonds can represent the total effect, then they should equal each other. That is, $F_{\mathrm{ext}}\Delta x_{\mathrm{r}}=\sum_{\mathrm{i}}^{\mathrm{N}} F_{\mathrm{FDA}}^{\mathrm{i}}\Delta x_{\mathrm{r}}^{\mathrm{i}}$ in all the cases, i is the index of the individual

bonds and N is the total number of bonds onto which the force distributes.

We assume that the contribution from a bond that contains hydrogen atom is negligible, and only consider the bonds formed within the carbon backbone of tDCB.

First, we consider $N = 1$. That is to find if the mechanical work primarily distributed onto a single bond. For all 15 bonds, we find no correlation of the total work $F_{\mathrm{ext}}\Delta x_{\mathrm{r}}$ with any $F^{\mathrm{i}}_{\mathrm{FDA}}\Delta x^{\mathrm{i}}_{\mathrm{r}}$, which indicates that the effect on a single bond cannot represent the total effect of the force.

Next, we considered $N = 2$, resulting in 105 combinations, out of which, Table S12 shows only the first 20 with lowest sum of squared residuals (ssResid). The combination of the work to bond CB-CE (index 8) and CB-CF (index 9) gave the highest correlation to the total work. However, the correlation is as low as 0.73, indicating that those two bonds only contribute part of the work.

Next, we considered $N = 3$, or 455 combinations. We found that the sum of work on bonds CA-CE (index 4), CB-CE (index 8) and CB-CF (index 9) exhibited a correlation of 0.89 with the total effect of force (Table S12, only the first 20 with the lowest ssResid are shown).

Taking one additional bond (N=4) into account (Table S12) did not improve the correlation, so that the three bonds identified above take up the significant portion of the external work.

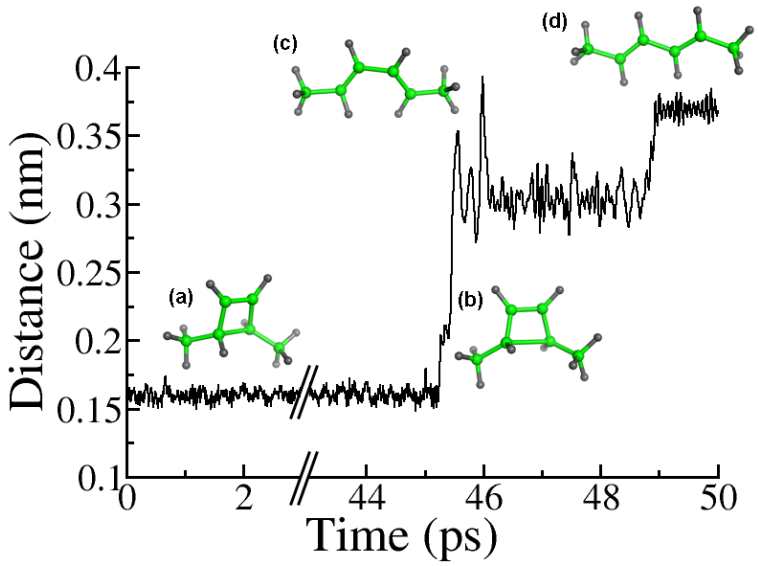

Fig. S1: **An example of a ring opening trajectory of tDCB under constant flooding potential.** Under a given constant flooding potential, the ring opening of tDCB can occur in 50 ps with high probability. Here, the distance between atoms CB and CE over time is shown. (a), (b), (c) and (d) are four representative structures during the ring opening and are taken at time of 2 ps, 45.4 ps, 47.5 ps and 49 ps, respectively.

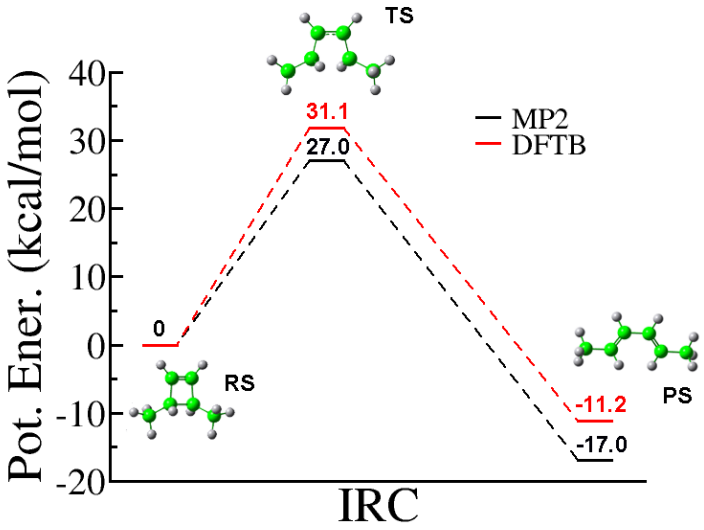

Fig. S2: Potential energies of the reactant state (RS), the transition state (TS), and the product state (PS) for the ring opening of tDCB estimated at the MP2/6-31+G (black) and SCC-DFTB (red) levels.

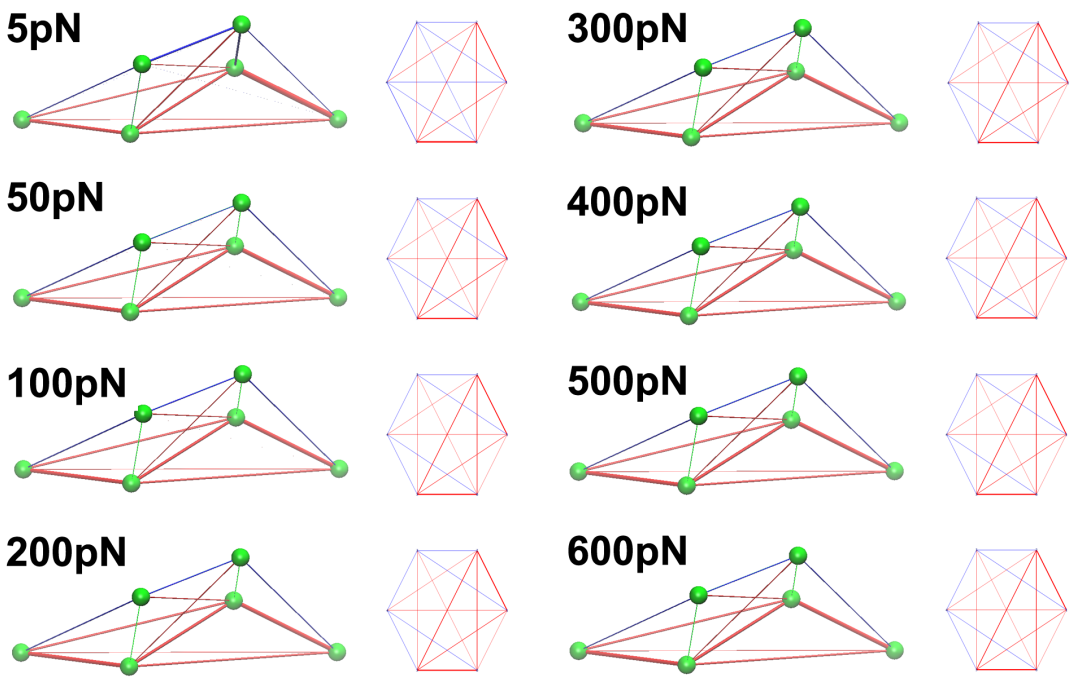

Fig. S3: **Force distribution within tDCB under constant forces.** The constant forces under which tDCB is pulled are shown in the upper-left corner of each structure. Left: Force distributions are superimposed on the 3D structure of tDCB. The pair-wise forces are represented by cylinders connecting atom pairs. The radius and the color of the cylinders indicate the magnitude and direction of the force, with blue for repulsive forces and red for attractive forces. All forces are normalized by the constant pulling force. Only the force distribution within the carbon backbone of tDCB is shown. Green atoms are the carbon atoms in tDCB and are labelled as in Fig. 1A of the main text. Right: Circle graph representations of the force distribution shown in the left. The labels around the circumference are the labels of carbon atoms in tDCB. Colors and line thickness indicate force magnitudes and directions, as in the representation on the left.

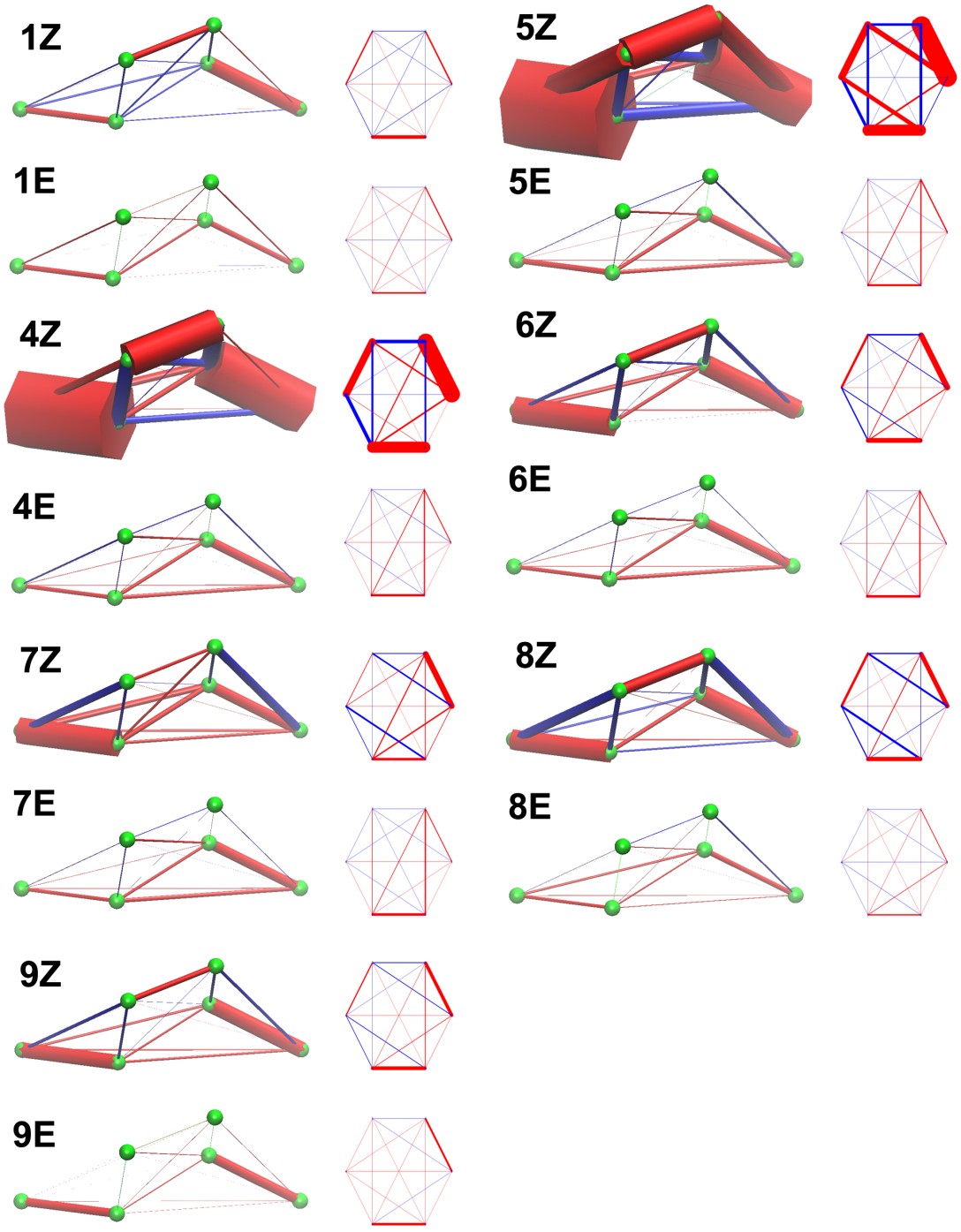

Fig. S4: **Force distribution within tDCB in macrocycles.** The labels of the macrocycles are shown in the upper-left corner of each structure. The details of the graphs see Fig. S3, here, the forces are normalized by the effective force that the macrocycle applies to tDCB.

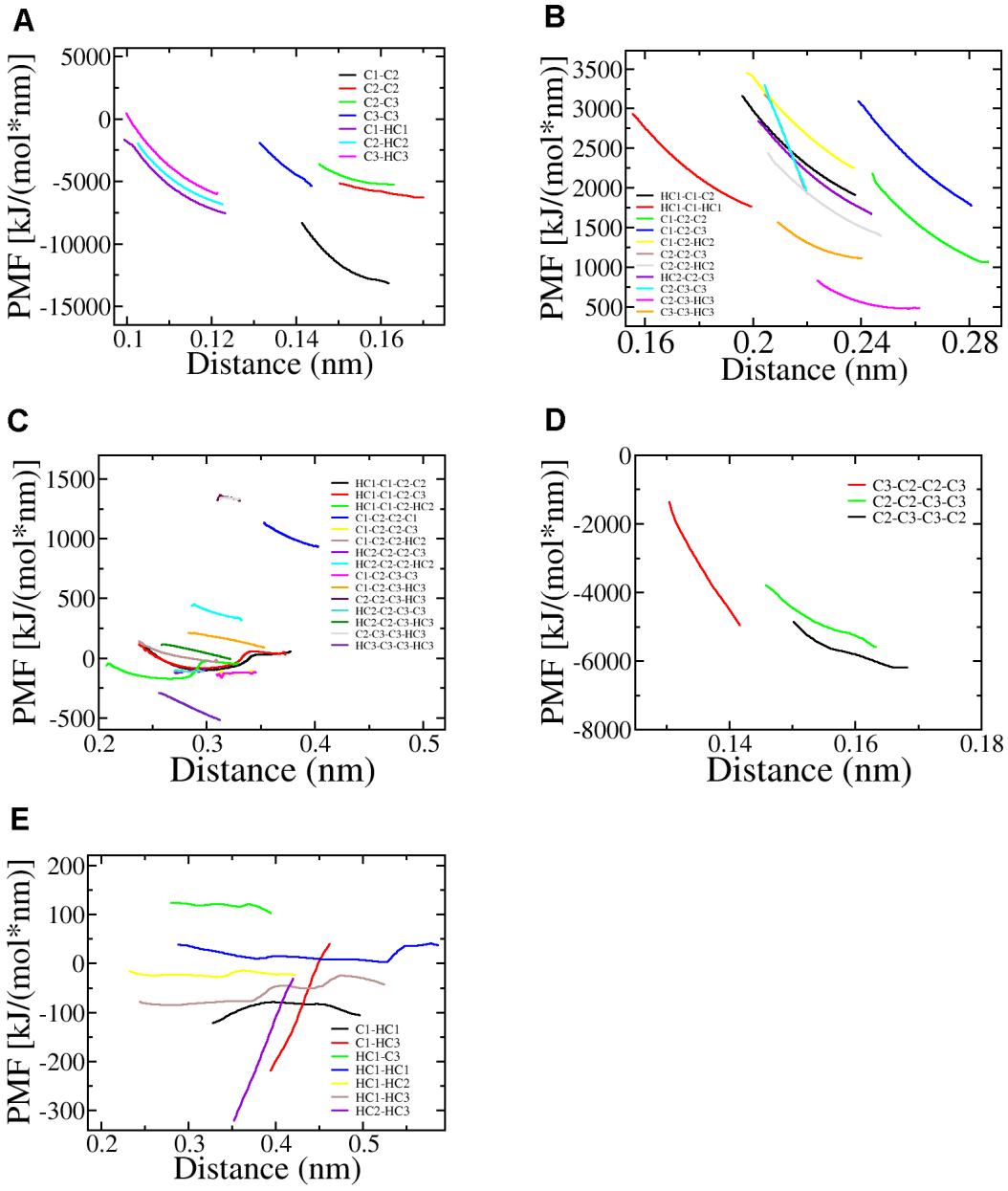

Fig. S5: **The tabulated potentials in the PWFF.** (A) 1-2 bonds; (B) 1-3 bonds; (C) and (D) 1-4 bonds; (E) non-bonded connections

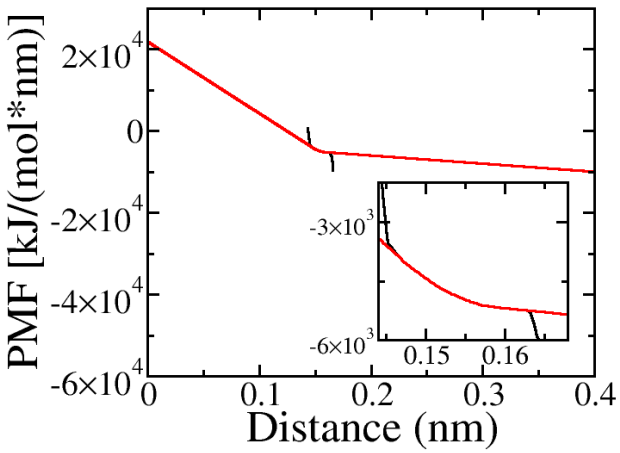

Fig. S6: **An example of the linear extrapolation of the tabulated potential in PWFF**. Here, we take the tabulated potential on the C2-C3 bond (black curve) as an example to show how we extrapolate to the range from 0 to a specific distance (red curve, the extrapolated potential). A linear potential is assumed for the range out of the essential distance.

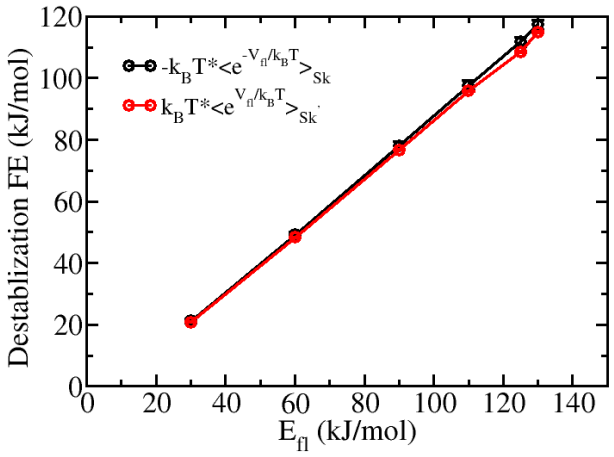

Fig. S7: **Consistency of the destabilization free energy obtained in two ensembles.**

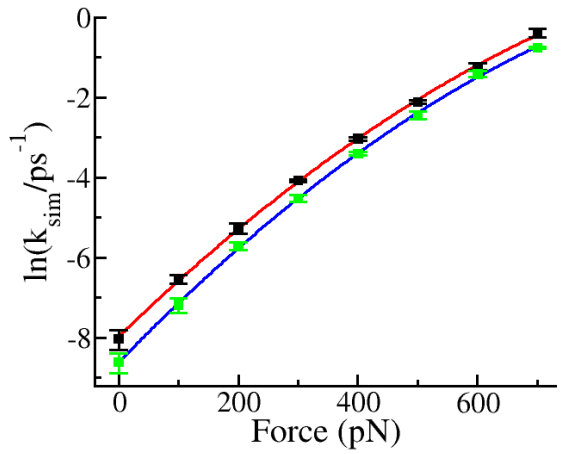

Fig. S8: **Force-dependent reaction rate of the ring-opening of tDCB.** The rates for the ring-opening of tDCB with a flooding strength of 130 kJ/mol (black squares) and 125 kJ/mol (green squares) are shown. Both of the rates are fitted to the Dudko-Hummer model (red and blue curves under flooding strengths of 130 kJ/mol and 125 kJ/mol, respectively).

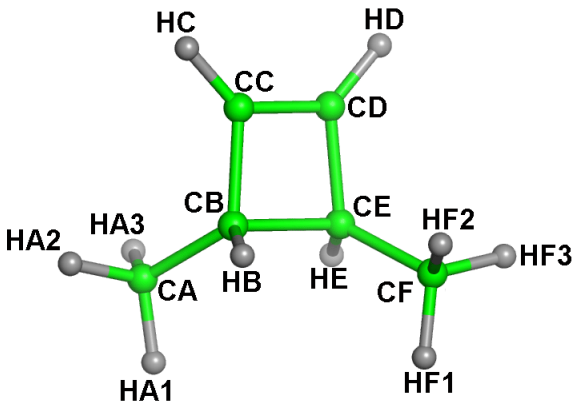

Fig. S9: **Atom names in tDCB.**

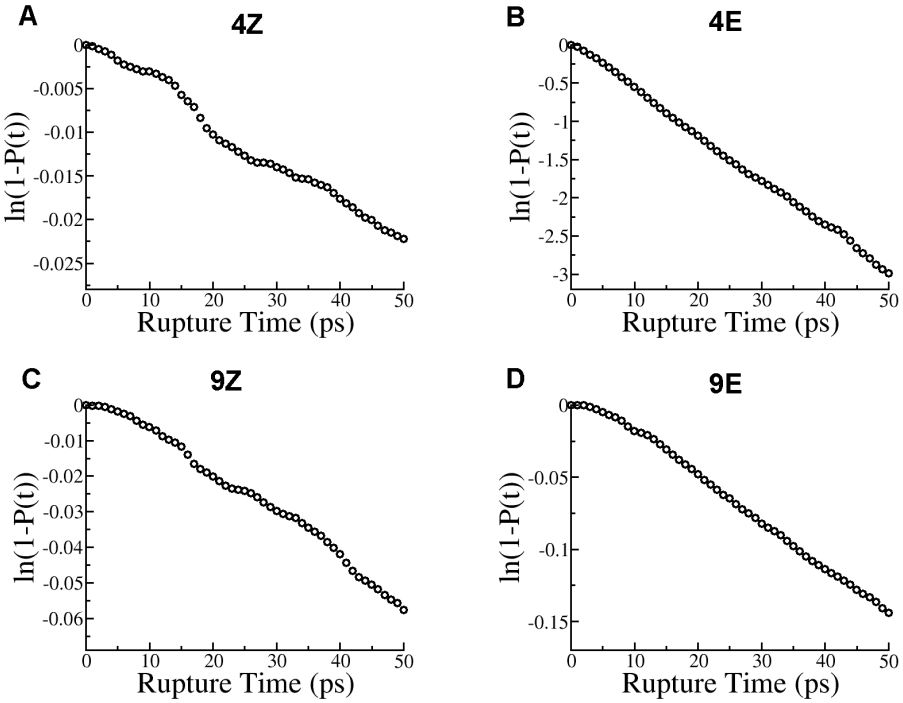

Fig. S10: **Rate estimations from conformational flooding.** $\ln(1 - P(t))$ as a function of t is shown in A, B, C, and D for 4Z, 4E, 9Z, and 9E, respectively.

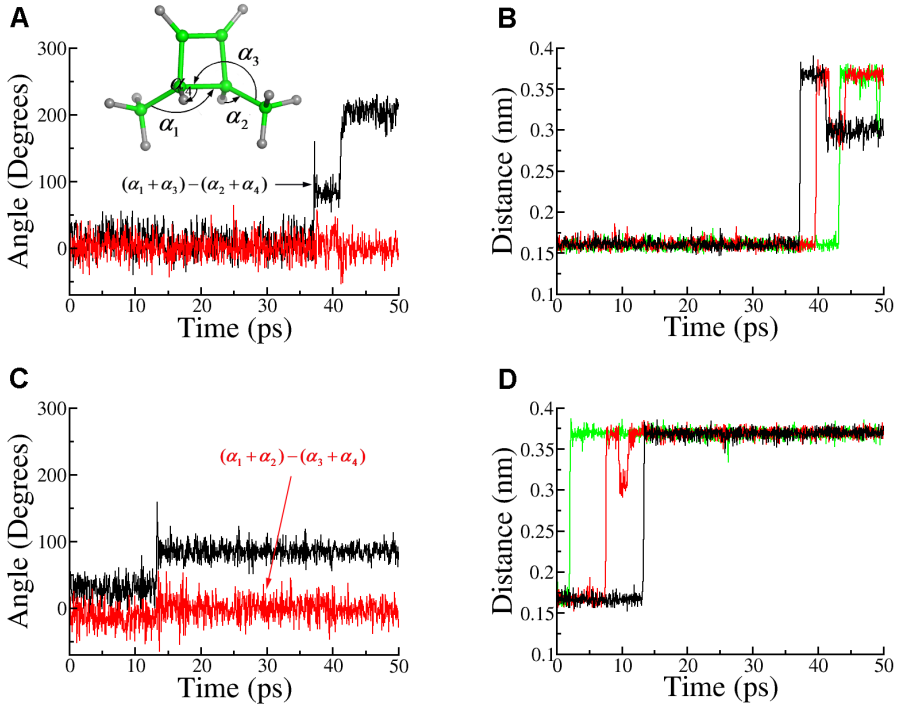

Fig. S11: **Conrotary ring opening.** Conrotatory ($(\alpha_1+\alpha_3)$-$(\alpha_2+\alpha_4)$) and disrotatory ($(\alpha_1+\alpha_2)$-$(\alpha_3+\alpha_4)$) angles are shown as a function of time in the case of 4Z (A) and 4E (C). The conrotatory angle increases dramatically in all the cases, indicating all rings to open in a conrotatory fashion. B and D are three representative examples in 4Z and 4E showing the distance of the CB-CE bond as a function of time. Rings open at different times. On average, the ring opens earlier in 4E than in 4Z.

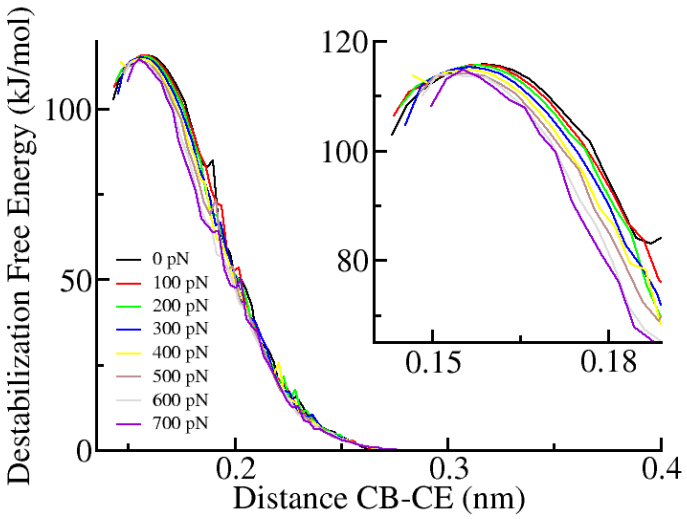

Fig. S12: **Destabilization free energies along the distance of CB-CE under constant pulling force.** The destabilization free energies are different under different pulling forces. In general, we observed that the bigger the constant pulling force, the lower the destabilization free energy, which explained the smaller acceleration obtained with conformational flooding as compared to the experimental data under the same force.

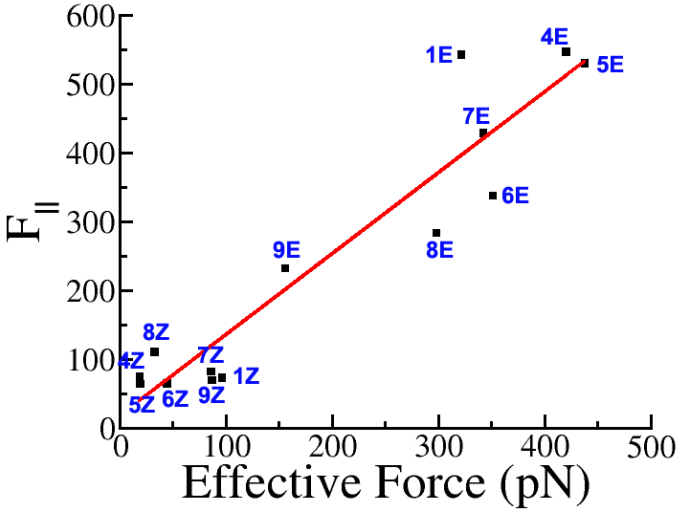

Fig. S13: Comparison between the effective force and the force along the $CH_3 \cdots CH_3$ axis ($F_{\|}$, as shown in Fig. 3b in Ref. [5]). The effective force and $F_{\|}$ correlate strongly. The linear fit (red) follows $y = 18.7 + 1.17x$, with a correlation coefficient of 0.95.

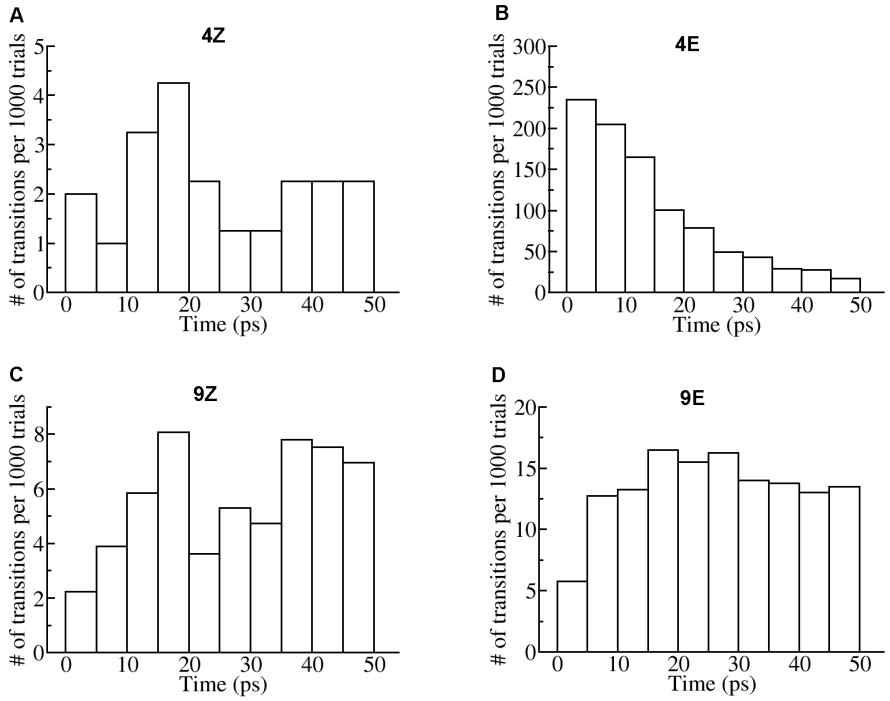

Fig. S14: **The distribution of the first passage times.** The number of rupture in 1000 trials as a function of t is shown in A, B, C, and D for 4Z, 4E, 9Z, and 9E, respectively.

Table S1: Number of trials and transitions, and estimated rates of the ring-opening in the case of tDCB under constant forces.

	125kJ/mol				130kJ/mol			
Force (pN)	# trials	# transitions	k (ps-1)	STD	# trials	# transitions	k (ps-1)	STD
0	4000	36	1.81E-04	4.30E-05	7600	123	3.26E-04	7.80E-05
100	4000	149	7.60E-04	1.37E-04	4000	279	1.44E-03	1.54E-04
200	2000	302	3.30E-03	3.47E-04	2000	453	5.13E-03	6.62E-04
300	2000	822	1.09E-02	8.56E-04	2000	1141	1.70E-02	5.25E-04
400	1000	778	3.30E-02	1.51E-03	1000	897	4.83E-02	2.00E-03
500	1000	973	8.68E-02	8.02E-03	1000	998	1.21E-01	4.99E-03
600	500	500	2.44E-01	1.61E-02	500	500	2.92E-01	2.44E-02
700	500	500	4.69E-01	8.84E-03	500	500	6.80E-01	7.57E-02

Table S2: Δx_{r} on individual bonds. We took structures of the RS and the TS from Ref. [5], which were optimized at the O3LYP/6-311G(2d,p) level. Then, Δx_{r} on each bond was obtained from the difference in bond length between TS and RS. Only Δx_{r}'s of atom pairs within the carbon backbone of the tDCB part were estimated. The structures used were the z-isomer(-), z-isomer(+), e-isomer(-) and e-isomer(+) of macrocycles 1, 4, 5, 6, 7, 8 and 9. Then, we averaged over all isomers of the macrocycles. The average Δx_{r} and its standard deviation (STD) are shown. Unit: Å

Δx_{r}	CB	CC	CD	CE	CF	STD	CB	CC	CD	CE	CF
CA	-0.015	-0.007	0.297	0.697	0.736	CA	0.007	0.032	0.043	0.032	0.057
CB		-0.087	0.118	0.563	0.709	CB		0.009	0.008	0.021	0.030
CC			0.033	0.113	0.306	CC			0.010	0.009	0.041
CD				-0.088	0.002	CD				0.009	0.033
CE					-0.018	CE					0.007

Table S3: Number of trials and transitions in the case of macrocycles.

Macrocycles	# trials	# transitions
1Z	3992	253
1E	1000	679
4Z	4000	88
4E	2000	1899
5Z	3600	78
5E	3000	2929
6Z	3876	124
6E	1930	1493
7Z	3000	167
7E	1500	1107
8Z	4000	108
8E	4000	2260
9Z	3590	201
9E	4000	537

Table S4: Force distributions within the tDCB under different forces estimated at the SCC-DFTB level. Averages over 10 trajectories are given in the left half of the table, standard errors of the mean (SEM) in the right half. All the forces are in the unit of pN.

5pN	CB	CC	CD	CE	CF	SEM	CB	CC	CD	CE	CF
CA	2.27	-0.75	-0.02	1.24	0.54	CA	1.55	0.21	0.02	0.28	0.05
CB		-0.35	1.02	1.58	1.59	CB		0.82	0.52	0.68	0.18
CC			-1.31	0.53	-0.02	CC			1.23	1.00	0.02
CD				-1.34	-0.64	CD				0.63	0.19
CE					3.69	CE					1.24
50pN	CB	CC	CD	CE	CF	SEM	CB	CC	CD	CE	CF
CA	28.09	-8.32	0.09	14.71	5.49	CA	1.08	0.34	0.02	0.25	0.06
CB		-1.32	6.72	18.06	15.06	CB		1.02	0.35	0.45	0.19
CC			-5.56	6.72	0.07	CC			0.90	1.05	0.02
CD				-1.71	-8.11	CD				0.61	0.37
CE					29.02	CE					0.96
100pN	CB	CC	CD	CE	CF	SEM	CB	CC	CD	CE	CF
CA	53.65	-16.69	0.14	29.14	10.84	CA	1.64	0.29	0.02	0.35	0.06
CB		-3.07	12.37	36.07	29.68	CB		1.09	0.69	0.79	0.24
CC			-16.41	13.49	0.13	CC			0.80	0.99	0.02
CD				-3.32	-16.25	CD				0.64	0.23
CE					56.07	CE					1.39
200pN	CB	CC	CD	CE	CF	SEM	CB	CC	CD	CE	CF
CA	111.13	-31.86	0.23	59.03	21.31	CA	1.04	0.24	0.02	0.29	0.06
CB		-5.16	28.36	73.27	59.03	CB		0.81	0.71	0.48	0.31
CC			-30.87	28.09	0.23	CC			1.29	1.04	0.02
CD				-5.99	-31.79	CD				0.70	0.25
CE					112.34	CE					1.64
300pN	CB	CC	CD	CE	CF	SEM	CB	CC	CD	CE	CF
CA	167.02	-46.60	0.28	88.17	31.35	CA	1.43	0.34	0.02	0.29	0.05
CB		-9.23	42.23	110.17	87.96	CB		0.81	0.48	0.49	0.26
CC			-41.20	42.17	0.28	CC			1.09	0.80	0.02
CD				-9.60	-46.91	CD				0.74	0.21
CE					166.22	CE					1.10
400pN	CB	CC	CD	CE	CF	SEM	CB	CC	CD	CE	CF
CA	222.50	-60.73	0.28	116.67	41.09	CA	1.13	0.34	0.02	0.29	0.04
CB		-11.54	56.30	147.32	116.87	CB		0.71	0.50	0.60	0.24
CC			-56.58	56.32	0.28	CC			1.09	0.90	0.02
CD				-13.52	-61.10	CD				0.69	0.33
CE					220.27	CE					1.46
500pN	CB	CC	CD	CE	CF	SEM	CB	CC	CD	CE	CF
CA	277.96	-73.93	0.24	145.55	50.58	CA	1.51	0.29	0.02	0.26	0.07
CB		-15.73	70.47	186.14	145.63	CB		0.90	0.76	0.42	0.27
CC			-71.66	71.09	0.23	CC			1.37	0.86	0.02
CD				-15.41	-73.88	CD				0.92	0.44
CE					277.30	CE					1.32
600pN	CB	CC	CD	CE	CF	SEM	CB	CC	CD	CE	CF
CA	336.19	-86.14	0.16	174.30	59.92	CA	1.52	0.22	0.02	0.28	0.05
CB		-20.06	85.42	224.26	174.30	CB		0.75	0.60	0.68	0.26
CC			-84.98	85.95	0.15	CC			1.40	0.81	0.03
CD				-20.39	-86.11	CD				0.71	0.36
CE					334.92	CE					1.75

Table S5: Force distributions within the tDCB under different forces estimated at the O3LYP/6-311G(2d,p) level. Averages over 10 trajectories are given in the left half of the table, standard errors of the mean (SEM) in the right half. All the forces are in the unit of pN.

5pN	CB	CC	CD	CE	CF	SEM	CB	CC	CD	CE	CF
CA	1.57	-1.89	0.00	-1.40	0.32	CA	3.98	2.69	0.17	2.44	0.43
CB		0.09	-3.12	-0.10	-0.26	CB		3.46	1.46	3.03	1.73
CC			7.48	3.02	0.11	CC			7.43	1.39	0.09
CD				3.44	-0.01	CD				4.07	1.39
CE					1.88	CE					4.43
50pN	CB	CC	CD	CE	CF	SEM	CB	CC	CD	CE	CF
CA	25.83	-6.92	-0.16	14.54	6.57	CA	5.40	2.50	0.18	2.02	0.47
CB		-1.60	1.02	21.27	14.17	CB		3.00	1.74	3.31	1.53
CC			1.15	5.73	0.05	CC			7.01	1.65	0.13
CD				4.28	-7.47	CD				3.61	1.65
CE					24.23	CE					3.03
100pN	CB	CC	CD	CE	CF	SEM	CB	CC	CD	CE	CF
CA	54.93	-11.88	-0.11	30.01	12.78	CA	3.98	2.33	0.16	1.91	0.48
CB		-3.69	7.04	38.46	29.30	CB		2.73	1.93	3.29	1.99
CC			-10.05	10.46	0.07	CC			5.71	2.38	0.15
CD				0.84	-12.76	CD				2.70	2.19
CE					52.79	CE					5.03
200pN	CB	CC	CD	CE	CF	SEM	CB	CC	CD	CE	CF
CA	102.87	-28.94	-0.24	60.97	24.65	CA	4.68	2.19	0.09	1.77	0.30
CB		-4.75	14.93	83.72	62.91	CB		1.76	2.15	4.88	1.60
CC			-18.04	20.59	0.12	CC			5.86	1.99	0.16
CD				-3.46	-25.20	CD				3.75	1.47
CE					109.67	CE					5.66
300pN	CB	CC	CD	CE	CF	SEM	CB	CC	CD	CE	CF
CA	157.27	-39.15	0.05	92.48	35.33	CA	5.13	1.99	0.21	1.33	0.58
CB		-8.97	25.18	127.52	91.36	CB		3.08	1.48	4.05	3.03
CC			-35.27	27.64	-0.09	CC			4.90	2.22	0.23
CD				-3.00	-41.56	CD				3.97	1.85
CE					155.82	CE					5.33
400pN	CB	CC	CD	CE	CF	SEM	CB	CC	CD	CE	CF
CA	209.52	-52.40	0.08	120.22	44.70	CA	5.28	2.12	0.16	2.55	0.48
CB		-12.94	35.38	165.66	116.94	CB		2.69	1.96	3.60	2.04
CC			-51.52	36.27	-0.16	CC			6.58	2.24	0.16
CD				-5.44	-54.85	CD				2.88	2.13
CE					205.92	CE					6.05
500pN	CB	CC	CD	CE	CF	SEM	CB	CC	CD	CE	CF
CA	260.38	-66.57	-0.25	150.18	52.83	CA	5.32	2.33	0.13	3.52	0.44
CB		-19.46	44.12	207.08	148.13	CB		2.59	1.58	5.42	3.26
CC			-58.26	43.98	0.31	CC			7.58	1.55	0.24
CD				-11.52	-65.17	CD				4.80	1.51
CE					254.36	CE					6.35
600pN	CB	CC	CD	CE	CF	SEM	CB	CC	CD	CE	CF
CA	307.28	-76.07	-0.13	179.34	60.07	CA	6.09	2.42	0.12	2.28	0.59
CB		-20.28	52.19	245.01	177.06	CB		2.69	1.66	4.57	2.36
CC			-74.37	55.66	-0.02	CC			4.91	2.11	0.13
CD				-20.19	-78.36	CD				2.81	1.29
CE					304.60	CE					4.43

Table S6: Linearity of the force distribution on individual bonds. The correlation between the force on the bond (x) and the external/effective force (y) are evaluated by the fit to equation y=ax. R and ssResid are the correlation coefficient and the sum of squared residuals, respectively. The correlation in complex number indicates a poor correlation. In the case of system A, forces on the individual bonds are highly correlated with the external force. Only the force on CA-CD and CC-CF have a lower correlation coefficient of 0.62 and 0.61, respectively, which is not surprise given their lower force values in these bonds. In the case of system B, only the forces on bonds CE-CF and CB-CE have high correlation coefficients of 0.89 and 0.87, respectively.

		tDCB under constant force			macrocycles		
index	Bond	a	ssResid	R	a	ssResid	R
1	CA-CB	1.79	27.77	1.00	0.85	282350	0.37
2	CA-CC	-6.73	1073.7	1.00	-1.99	699900	0+1.0644i
3	CA-CD	1484.9	2.05E+005	0.62	70.30	529280	0+0.78288i
4	CA-CE	3.43	17.96	1.00	3.29	551960	0+0.82585i
5	CA-CF	9.84	359.35	1.00	7.01	197020	0.63
6	CB-CC	-31.67	3940.1	0.99	-4.96	343130	0+0.21362i
7	CB-CD	7.08	192.85	1.00	6.75	567220	0+0.85353i
8	CB-CE	2.69	56.64	1.00	2.26	81553	0.87
9	CB-CF	3.43	20.74	1.00	1.64	204130	0.61
10	CC-CD	-7.02	793.25	1.00	-0.84	815280	0+1.2184i
11	CC-CE	7.04	87.57	1.00	3.38	148310	0.74
12	CC-CF	1520.8	2.08E+005	0.61	-44.09	741600	0+1.1225i
13	CD-CE	-30.46	3169.4	1.00	-0.32	851050	0+1.2623i
14	CD-CF	-6.73	1102.7	1.00	-2.16	567320	0+0.85372i
15	CE-CF	1.8	35.2	1.00	0.69	68868	0.89

Table S7: Force distribution in the z-isomers of macrocycles at the SCC-DFTB level. All the forces are in the unit of pN.

1Z	CB	CC	CD	CE	CF	SEM	CB	CC	CD	CE	CF
CA	99.51	-19.34	1.86	-31.80	0.32	CA	4.92	3.80	0.10	4.57	1.36
CB		-27.47	-26.17	-22.98	-15.40	CB		2.57	1.60	2.70	1.30
CC			96.12	-11.56	0.57	CC			2.15	1.84	0.30
CD				-33.47	17.96	CD				1.32	11.18
CE					226.02	CE					21.99
4Z	CB	CC	CD	CE	CF	SEM	CB	CC	CD	CE	CF
CA	218.88	20.52	-0.82	22.47	1.68	CA	6.88	3.29	0.14	2.72	0.91
CB		-42.24	-2.72	14.79	-19.72	CB		0.75	1.16	1.42	1.46
CC			95.86	-21.49	0.61	CC			1.83	1.12	0.13
CD				-46.04	5.48	CD				0.89	3.74
CE					146.98	CE					3.43
5Z	CB	CC	CD	CE	CF	SEM	CB	CC	CD	CE	CF
CA	260.94	71.09	-2.43	23.01	-9.43	CA	5.63	6.25	0.30	4.26	1.00
CB		-30.81	-5.78	-0.29	-36.92	CB		2.11	1.86	2.33	2.01
CC			96.62	-29.68	-0.65	CC			1.89	1.36	0.14
CD				-39.62	56.69	CD				1.86	4.79
CE					152.71	CE					2.99
6Z	CB	CC	CD	CE	CF	SEM	CB	CC	CD	CE	CF
CA	188.33	-23.56	0.33	31.79	11.67	CA	13.07	7.26	0.41	7.47	1.96
CB		-42.47	-2.69	22.02	0.78	CB		3.04	2.88	2.64	8.85
CC			74.38	-14.76	1.30	CC			3.52	2.32	0.24
CD				-41.21	-27.90	CD				1.09	9.62
CE					141.24	CE					8.13
7Z	CB	CC	CD	CE	CF	SEM	CB	CC	CD	CE	CF
CA	355.35	-92.80	1.88	85.38	35.66	CA	4.77	1.95	0.07	4.34	1.04
CB		-37.84	32.45	66.53	41.86	CB		0.68	2.15	3.89	2.86
CC			38.43	-5.10	3.36	CC			3.18	1.90	0.04
CD				-36.01	-108.07	CD				1.03	2.15
CE					146.17	CE					2.42
8Z	CB	CC	CD	CE	CF	SEM	CB	CC	CD	CE	CF
CA	104.98	-44.54	2.35	-11.40	7.45	CA	2.17	7.56	0.28	2.89	1.78
CB		-25.88	0.68	19.08	-9.86	CB		0.92	1.39	3.06	2.83
CC			57.60	-3.82	2.48	CC			3.05	1.18	0.28
CD				-25.70	-51.09	CD				0.82	8.40
CE					95.84	CE					3.83
9Z	CB	CC	CD	CE	CF	SEM	CB	CC	CD	CE	CF
CA	205.84	-40.93	1.22	33.40	18.67	CA	5.89	2.00	0.12	2.70	0.59
CB		-35.12	-3.64	24.50	32.59	CB		1.14	1.24	2.43	2.46
CC			72.63	-3.24	1.21	CC			1.77	1.52	0.11
CD				-35.37	-39.64	CD				1.31	2.25
CE					211.02	CE					5.25

Table S8: Force distribution on the e-isomers(-) of macrocycles at the SCC-DFTB level. All the forces are in the unit of pN.

1E	CB	CC	CD	CE	CF	SEM	CB	CC	CD	CE	CF
CA	264.07	73.02	-1.02	1.75	-4.35	CA	2.12	1.10	0.08	1.64	0.32
CB		-12.97	39.92	100.99	5.28	CB		0.88	0.46	1.12	2.34
CC			17.85	40.92	-1.12	CC			2.16	0.59	0.10
CD				-12.20	73.53	CD				0.69	1.53
CE					265.20	CE					2.46
4E	CB	CC	CD	CE	CF	SEM	CB	CC	CD	CE	CF
CA	271.65	-103.59	4.44	44.47	59.43	CA	1.21	1.39	0.05	0.52	0.42
CB		-58.23	21.48	203.08	258.44	CB		0.50	0.33	1.43	1.14
CC			-61.81	132.86	-1.88	CC			1.76	1.52	0.05
CD				16.14	-94.83	CD				0.89	2.04
CE					598.47	CE					1.55
5E	CB	CC	CD	CE	CF	SEM	CB	CC	CD	CE	CF
CA	391.03	-39.27	4.19	19.26	58.03	CA	19.08	10.88	0.13	5.76	0.50
CB		-45.20	45.95	227.30	270.44	CB		1.85	4.12	4.68	4.02
CC			-48.01	131.78	-0.90	CC			4.46	1.34	0.19
CD				-1.57	-138.84	CD				1.90	10.19
CE					560.77	CE					8.48
6E	CB	CC	CD	CE	CF	SEM	CB	CC	CD	CE	CF
CA	219.95	-30.87	1.23	36.97	43.27	CA	1.20	0.38	0.02	0.52	0.08
CB		-56.31	-5.11	137.41	217.36	CB		0.55	0.50	0.65	0.23
CC			-32.00	102.69	-3.37	CC			2.45	0.78	0.02
CD				11.72	-31.94	CD				0.63	0.46
CE					547.84	CE					1.02
7E	CB	CC	CD	CE	CF	SEM	CB	CC	CD	CE	CF
CA	198.87	-28.55	1.36	27.47	42.32	CA	1.24	0.35	0.02	0.37	0.09
CB		-56.61	-7.40	135.52	220.31	CB		0.55	0.53	0.53	0.27
CC			-33.21	104.87	-3.47	CC			2.06	0.70	0.02
CD				13.83	-33.66	CD				0.79	0.38
CE					542.53	CE					1.13
8E	CB	CC	CD	CE	CF	SEM	CB	CC	CD	CE	CF
CA	152.52	-14.46	-1.16	107.63	28.19	CA	9.65	15.04	0.77	6.88	1.62
CB		-3.47	12.72	62.25	37.99	CB		1.23	4.34	4.36	6.76
CC			-28.62	35.63	2.32	CC			0.98	1.77	0.33
CD				-4.25	-71.90	CD				1.42	7.53
CE					228.77	CE					4.76
9E	CB	CC	CD	CE	CF	SEM	CB	CC	CD	CE	CF
CA	210.52	-0.36	1.28	-0.54	7.20	CA	9.28	6.12	0.34	5.77	1.33
CB		-6.10	7.06	24.29	6.43	CB		2.87	2.66	4.01	8.08
CC			4.06	16.07	0.84	CC			1.42	4.64	0.24
CD				3.15	10.59	CD				3.94	4.39
CE					238.47	CE					15.59

Table S9: Definition of atom types used in MSCGFM. The atom names are shown in Fig. S9.

CG sites	atoms
C1	CA CF
HC1	HA1 HA2 HA3 HF1 HF2 HF3
C2	CB CE
HC2	HB HE
C3	CC CD
HC3	HC HD

Table S10: Destabilization free energy obtained in two ensembles. All numbers are in the unit of kJ/mol.

E_{fl}	-$\mathrm{k_B T}\cdot\ln\langle e^{-\mathrm{V_{fl}/kT}}\rangle_{\mathrm{sk}}$	STD	$\mathrm{k_B T}\cdot\ln\langle e^{\mathrm{V_{fl}/kT}}\rangle_{\mathrm{sk'}}$	STD
30	21.18	0.62	20.88	0.19
60	49.13	1.11	48.28	0.21
90	78.09	1.39	76.72	0.12
110	97.65	1.52	95.84	0.12
125	111.79	1.58	108.51	0.24
130	117.31	1.61	114.99	0.35

Table S11: Mechanical parameters obtained from the Dudko-Hummer fit.

Flooding strength (kJ/mol)	Δx_{r} (Å)	$\Delta G^{\ddagger}$ (kJ/mol)
125	0.66	28.4
130	0.62	28.7

Table S12: Fitting to y=x with the sum of the work on two, three and four bonds. Only the first 20 with lowest sum of squared residuals (ssResid) are shown.

Two bonds				Three bonds					Four bonds					
Index		ssResid	R	Index			ssResid	R	Index				ssResid	R
8	9	1719	0.73	4	8	9	785.72	0.89	4	7	8	9	747.79	0.89
4	9	2250.9	0.63	5	8	9	1294.8	0.81	4	8	9	11	748.82	0.89
4	8	2707	0.52	8	9	11	1595.6	0.76	4	8	9	13	769.9	0.89
5	9	3195.5	0.38	7	8	9	1609.5	0.75	4	6	8	9	774.53	0.89
5	8	3528.9	0.23	4	5	9	1609.5	0.75	4	5	8	9	774.93	0.89
9	11	3949.9	0+0.2422i	6	8	9	1680.8	0.74	4	8	9	12	785.26	0.89
7	9	4050	0+0.29239i	8	9	13	1686.1	0.74	4	8	9	14	785.56	0.89
6	9	4158.3	0+0.33842i	2	8	9	1713.9	0.74	4	8	9	10	785.93	0.89
9	13	4206.7	0+0.35708i	8	9	12	1716.9	0.73	2	4	8	9	786.07	0.89
2	9	4238.1	0+0.36866i	3	8	9	1718	0.73	3	4	8	9	786.51	0.89
3	9	4241.3	0+0.36981i	8	9	14	1720.6	0.73	1	4	8	9	826.55	0.88
9	12	4251.5	0+0.3735i	8	9	10	1736.6	0.73	4	8	9	15	849.25	0.88
9	14	4254.5	0+0.37456i	1	8	9	1811.5	0.72	5	7	8	9	1216.2	0.82
9	10	4295.5	0+0.38898i	8	9	15	1851.4	0.71	5	8	9	11	1235	0.82
8	11	4416.6	0+0.42867i	4	5	8	1859.4	0.71	5	8	9	13	1266.4	0.81
1	9	4421.6	0+0.43022i	4	9	11	2037	0.67	5	6	8	9	1277.8	0.81
9	15	4517.9	0+0.45924i	4	7	9	2122.1	0.66	5	8	9	12	1292	0.81
7	8	4588	0+0.47926i	4	6	9	2185.9	0.64	2	5	8	9	1292.9	0.81
6	8	4676.5	0+0.50341i	4	9	13	2224.4	0.64	5	8	9	14	1295.3	0.81
8	13	4758.1	0+0.52468i	3	4	9	2243.7	0.63	3	5	8	9	1297.3	0.81

Table S13: The potential energies and geometrical parameters for the RS, TS, and PS shown in Fig. S2.

	Potentail Energy (kcal/mol)		Distance CB-CE (nm)	
Structures	MP2	SCC-DFTB	MP2	SCC-DFTB
RS	0.0	0.0	0.161	0.157
TS	27.0	31.1	0.217	0.211
PS	-17.0	-11.2	0.315	0.302

References

[1] Lu, L.; Izvekov, S.; Das, A.; Andersen, H.; Voth, G. *J. Chem. Theory Comput.* **2010**, *6*, 954–965.

[2] Elstner, M.; Porezag, D.; Jungnickel, G.; Elsner, J.; Haugk, M.; Frauenheim, T.; Suhai, S.; Seifert, G. *Phys. Rev. B* **1998**, *58*, 7260–7268.

[3] Grubmüller, H. *Phys. Rev. E* **1995**, *52*, 2893–2906.

[4] Lange, O.; Schäfer, L.; Grubmüller, H. *J. Comput. Chem.* **2006**, *27*, 1693–1702.

[5] Yang, Q.; Huang, Z.; Kucharski, T.; Khvostichenko, D.; Chen, J.; Boulatov, R. *Nat. Nanotechnol.* **2009**, *4*, 302–306.

[6] *"LS-DYNA keyword users manual",* Version 971, *Livermore Software Technology Corporation,* Livermore California, **September 2006**.

[7] Belytschko, T.; Schwer, L.; Klein, M. *International Journal for Numerical Methods in Engineering* **1977**, *11*, 65–84.